



***In-situ* Synthesis of Cupric Oxide Nanoplates in Chitosan Matrix**

ELBRIGHT DILLU^{1*} and SAIMA HABIB KHAN¹

¹Department of Chemistry, Sam Higginbottom University of Agriculture, Technology and Sciences, Prayagraj-211007, Uttar Pradesh, India.

*Corresponding author E-mail: elbrightdillu@gmail.com

<http://dx.doi.org/10.13005/ojc/410136>

(Received: October 26, 2024; Accepted: January 11, 2025)

ABSTRACT

Metal oxide nanoparticles of different morphologies have been explored for their varied applications. Nanoplates of copper oxide, in particular, have been known to show better performance in sensing applications, but most methods reported for their preparation either involve toxic chemicals as stabilizers or high energy consumption. Chitosan, a derivative of chitin, has been extensively used as a stabilizer for different metal oxide based nanoparticles, and thus has been deemed as an eco-friendly approach towards the stabilization of nanoparticles. Keeping this in view, this article reports the preparation of cupric oxide nanoplates at ambient temperature synthesized inside chitosan matrix using *In-situ* approach. The product has been characterized using UV-Visible spectroscopy, SEM, FTIR, XRD and HR-TEM. The results indicate the successful formation of the aimed nanomaterial, based on which the optical, morphological, and crystal properties have been discussed.

Keywords: CuO nanoparticles, Nanocomposite, Chitosan, SEM, HRTEM, UV-Vis, FTIR, XRD.

INTRODUCTION

The term nanocomposite encompasses materials with either one or more phases carrying a nanodimensional structure. This type of material has been of particular interest to researchers especially because the desirable properties of two or more materials can be combined to meet new challenges and explore new applications. Besides that, emergence of new properties have also been reported in the resultant nanocomposites which were otherwise absent in the parent materials.¹ The utilization of chitosan in this field has, particularly, gained interest due to its inherent advantageous attributes, making it a preferred matrix

for this purpose. Chitosan is known, not only as a stabilizing matrix for nanoparticles, thus preventing nanoparticle growth, but also has been known for its aid in the reduction of metal ions during the synthesis of metal nanoparticles.²

Metal oxide nanoparticles possess several interesting properties which make them useful in several applications. Several metal oxide nanoparticles of the first transition series element have been reported to exhibit useful properties such as antibacterial, antioxidant, and photocatalysis.^{3,4,5,6} Among these, some metal oxide nanoparticles including those of copper oxide, exhibit semiconductor properties, which are valuable in



cutting-edge applications such as photocatalysis, sensing, superconductivity, photovoltaics, solar energy systems, lithium-ion batteries, and medical diagnostics. They represent a uniqueness of their own quite unlike the semiconductor materials used conventionally because of their charge transport nature, which usually involves a transfer of electronic charge from ns orbital of the metal to 2p orbital of oxygen. Furthermore, a low value of electron effective mass is an important reason why metal oxides act as better semiconductors than the conventional ones.⁷ As a result, there has been significant interest in exploring synthetic methods for the production of cuprous and cupric oxide nanoparticles. CuO nanoparticles, in particular, are identified as semiconductors of p-type, and their key characteristics, both physical and chemical, are being extensively studied.⁸ Additionally, recent studies highlight that the quantum confinement present in the case of electrons, or for the electron-hole pairs affects the interaction between light and matter. In semiconductor nanoparticles, this exciton confinement enables significant property modifications through band gap engineering.⁹

Moreover, copper has been a cost-effective antibacterial agent for a long time, and recently, the synthesis of copper oxide nanoparticles, either in the +1 or +2 state of copper, has received much attention from researchers worldwide. This is because of their newly discovered applications corresponding to their antidiabetic, anticancer, and antioxidant properties, besides the well-known antibacterial properties. Also since metallic nanoparticles of silver and gold have been extensively explored despite their high cost of production while copper oxide nanoparticles remain still less popular, they have been brought to trend.^{10,11} Since the synthesis of copper oxide nanoparticles faces the challenge of faster agglomeration due to their high surface energy, a wide variety of stabilizing agents, capping agents or surfactants have been employed, such as polyacrylic acids, poly(styrene sulphonate), daxad 19 etc. But the utilization of most of such surfactants do not contribute to an environment-friendly pathway, rather most of the times they bring ill effects to the environment. On the other hand, chitosan, a derivative of a biopolymer obtained from crustaceans is biocompatible, shows non-toxic behaviour towards animal cells in concern, and has additional advantages over its competitors due to the presence of polar groups like $-NH_2$ and

$-OH$ which can effectively interact with metal, and prevent agglomeration, and also because of its biodegradable nature.¹³ This is why chitosan-copper oxide nanocomposite deserves more research details both in the area of synthetic routes and characterization of the resultant nanocomposite so that new prospects can be envisioned for this nanocomposite.

When it comes to the morphology of nanoparticles, nanoplates in general have been interesting structures because of greater anisotropy compared to other nano-structured materials. Metal nanoplates, typically of noble metals, have been extensively studied and their role in understanding the self assembly of nanoparticles resulting hierarchical nano-objects have been sufficiently reviewed.¹⁴ On the other hand metal oxide nanoplates have been less explored; still, among the ones that have been synthesized, CuO nanoplates have been reported as one of the best alternatives among CuO nanomaterials of different morphologies, especially in the area of chemical sensing. Nanoplates of CuO have been found to exhibit excellent sensing properties towards ethanol, methanol, ethyl acetate, toluene, and many such chemicals. A comparison of CuO nanoplates with other morphologies of CuO nanoparticles has been experimented with and reported by different workers. The hierarchical structures formed by nanoplates have shown even better performance in the field of sensing.^{15,16}

This makes CuO nanoplate structures of special interest and therefore finding synthetic routes leading to the synthesis of such 2D nano-shape becomes particularly important. There have been many different methods through which nanoparticles of this morphology have been synthesized. Several researchers have reported chitosan CuO nanoparticles but mostly through the dispersion of separately formed CuO nanoparticles in chitosan,^{17,18} however, there have not been reports of *in-situ* room temperature synthesis of such structures with chitosan or similar biodegradable and non-toxic polymer as stabilizer, to the best of our knowledge. This paper reports facile, *in-situ*, ambient-temperature synthesis of chitosan-stabilized CuO nanoplates and its characterization using Ultraviolet-visible spectrum (further analysis of optical properties is shown through Tauc plot), FTIR analysis has been done to study the interaction of different functional groups with cupric ions,

and the crystal nature and morphology has been elucidated using sophisticated techniques like X-ray diffractometry, Electron microscopic techniques, and electron diffraction patterns (SAED). The energy dispersive spectrum has also been provided for further verification.

EXPERIMENTAL

Materials

Chitin (CH), Copper sulphate pentahydrate, sodium hydroxide, and glacial acetic acid used in this synthetic route were obtained from Merck.

Preparation of colloidal chitosan solution

Chitin flakes were dry grounded and soaked in 1M sodium hydroxide solution for 24 h, the resultant was centrifuged, and the precipitate was repeatedly treated with 50% sodium hydroxide to ensure a maximum degree of deacetylation in the chitosan.¹⁹ Finally the chitosan so obtained was washed multiple times with water to free the mixture of any remaining alkali and vigorously stirred with 1% acetic acid solution to prepare a colloidal chitosan solution.²⁰ Samples of dried chitin and chitosan were sent for FTIR analysis.

In-situ fabrication of copper oxide nanoplates inside chitosan (CS-CuO)

50 mM solution of copper sulphate was prepared, added to the chitosan solution and agitated using a magnetic stirrer at a speed of 200 rpm for 15 min at ambient temperature conditions to obtain a light blue homogeneous mixture. The pH of this solution was elevated to 10 using aqueous NaOH solution, and further, it was agitated at 500 rpm for 30 min at room temperature while the colour of the solution turned to dark brown due to the formation of CuO inside the chitosan matrix which precipitated due to its insolubility at this pH.^{21,13} This mixture was left overnight for complete precipitation and then centrifuged at 7000 rpm to separate the precipitate from the mother liquor. The obtained precipitate was washed with double distilled water, which was followed by ethanol washing to remove as much humidity as possible, and dried at 60°C before characterization.

Characterization

The nanocomposite (CS-CuO) was analyzed by carrying out several characterization

techniques, including XRD, UV-Visible spectroscopy, FTIR, SEM (with EDS), High-resolution TEM, and SAED. For UV-Visible analysis, a small portion of the precipitate was dispersed in water and scanned across wavelengths ranging from 200 nm to 750 nm. A spectrophotometer of Shimadzu® UV-VIS NIR (UV-3600 Plus model) was employed for this purpose. The wavelength vs. absorbance data obtained was plotted using Origin software, followed by Tauc plot, for the study of optical properties. FTIR spectra were obtained with a Perkin Elmer-Spectrum RX-I FTIR instrument, covering wave numbers from 400 cm⁻¹ to 4000 cm⁻¹. KBr pellets were prepared by finely grinding and mixing each of the samples separately (CH, CS, and CS-CuO) with KBr, then pressing them to form separate pellets before exposure to IR radiation. X-ray diffraction of the nanocomposite was carried out on a RIGAKU Smart® lab 3kW X-ray Diffractometer, within a scan range from 20° to 80° Bragg's angle and a fixed step size of 0.02 s; the scan speed for this analysis was set for 10° per minute. Electron microscopy was performed using JEOL JSM-7600F FEG-SEM for SEM images and JEOL JEM-2100F for TEM and SAED patterns. High-resolution TEM images were captured with a 200 kV accelerating voltage. For TEM imaging, the sample was dispersed in ultrapure water by ultrasonication for 15 min and the resultant dispersion was drop-cast onto a TEM grid. For SEM, the sample was placed directly on the sample holder, and secondary electron imaging was used for observation.

RESULTS AND DISCUSSION

UV-Visible spectral studies

The plot between wavelength and absorbance within the UV-Visible electromagnetic range has been shown in Fig.1a. The curve plotted between 250 nm to 700 nm shows a typical peak for CuO nanoparticles at 255.5 nm, which is accompanied by a shoulder between 320 nm and 400 nm. The sharp peak at 255.5 nm is assigned to the electronic transitions due to CuO nanoparticles where as the latter one corresponds to the surface plasmon resonance exhibited by CuO nanoparticles.²² For the determination of optical band gap, Tauc plots were obtained for both direct and indirect transition, which are shown in Fig. 1b and 1c, respectively. For direct transition, the formula $(\alpha h\nu)^2 =$

$A(h\nu - E_g)$ was used whereas $(\alpha h\nu)^{0.5} = A(h\nu - E_g)$ was used for indirect transition. Here α denotes absorption edge, A is a constant independent of frequency ν , the term ' $h\nu$ ' denotes the energy photon absorbed by the material, and E_g is the symbol used for the band gap of the material.²³ The band gaps were found by extrapolation of the curves between $(\alpha h\nu)^n$ and energy towards the x-axes, in either of the plots; the direct transition band gap as shown by the plot is 3.83 eV, which is greater than the bulk value for the same (3.5eV), whereas the indirect band gap is 2.34 eV. A comparison between the two band gaps verifies the crystalline nature of the material. Since the direct band gap is greater than the indirect one, the CuO phase is crystalline.²⁴ Since the indirect band gap suggests that this material is an indirect semiconductor, it can be said that there exists a difference of momentum between holes existing in the valence band and electrons in the conduction band. A radiative recombination is still achievable through alternate choices for the compensation of momentum such as phonons created through crystal lattice vibrations.²⁵

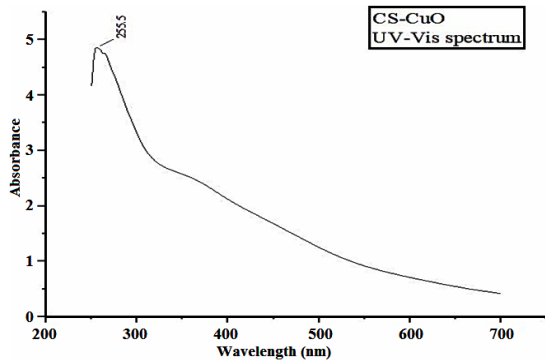


Fig. 1(a). UV-Visible wavelength vs. absorbance plot for the synthesized CS-CuO nanocomposite

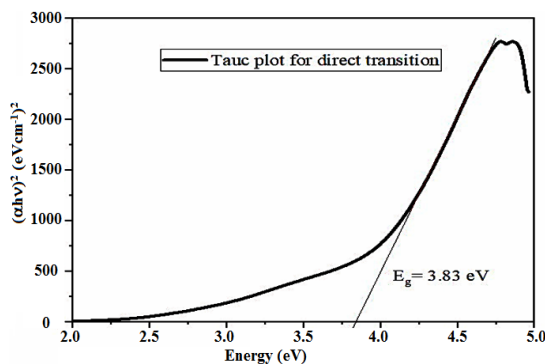


Fig. 1(b). Tauc plot for direct transition in the synthesized CS-CuO nanocomposite

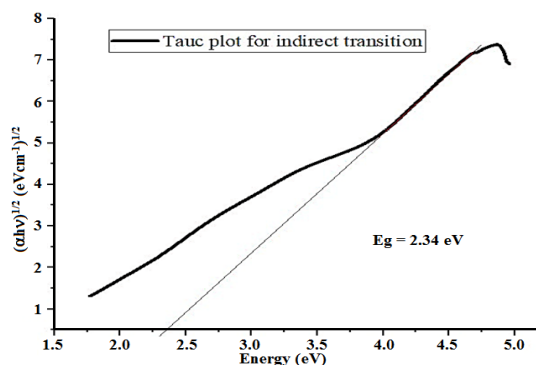


Fig. 1(c). Tauc plot for indirect transition in the synthesized CS-CuO nanocomposite

FTIR analysis

The comparative FTIR analyses of chitin (CH), chitosan (CS), and CS-CuO-NC clearly indicate the deacetylation of chitin for the formation of chitosan and subsequent formation of the aforementioned nanocomposite.

FTIR spectrum of chitin (Fig. 2) shows transmittance peaks at 1621 cm^{-1} along with 1655 cm^{-1} corresponding to $>\text{C}=\text{O}$ stretching frequencies, the former wavenumber being the one arising from the carbonyl group interacting with a neighbouring N-H bond through H-bonding, while the latter relating to the carbonyl group similarly hydrogen bonded to $-\text{OH}$ group of the residue present adjacent to it in the same chain. These peaks along with other peaks at 1310 cm^{-1} and 1552 cm^{-1} which correspond to C-N stretching and N-H bending frequencies, respectively, indicate that the chitin used for this synthesis has an α -conformation. Furthermore, the shift of the peak at 1552 cm^{-1} to 1562 (in chitosan) is due to deacetylation.^{26,27,28} The degree of deacetylation was calculated using absorbance data as derived from the transmittance in FTIR plot, and it was found to be around 75%. We have published the discussion of this part elsewhere in detail.²⁹

The FTIR transmittance spectrum of the CS-CuO nanocomposite shows a broad band between $3000\text{--}3500\text{ cm}^{-1}$ due to the overlapping $-\text{OH}$ and $-\text{NH}$ bond frequencies, and also suggests that these groups are hydrogen bonded to other polar groups in the vicinity. This peak has undergone further broadening as compared to the similar one in chitosan suggesting that the concerned bonds are interacting with each other, with nanoparticles, and

the water molecules adsorbed in the sample through hydrogen bonding. A shoulder-like peak above between 1600-1650 cm^{-1} can also be observed which could be due to H-O-H bending vibrations coming from the water molecules adsorbed on the surface of nanoparticles or on chitosan. The peak at 1556 cm^{-1} represents the bending vibrations of the amide. The bending vibration in the $-\text{CH}_3$ group of amide can be seen near 1405 cm^{-1} . The peaks at 1049 cm^{-1} , and 1027 cm^{-1} as assigned to stretching frequencies of the carbon-oxygen bond of the primary hydroxyl on C6 and the secondary hydroxyl group on C3 respectively. The peaks observed between 800 cm^{-1} and 1000 cm^{-1} represent CH bending vibrations, whereas the peaks below 700 are due to Cu-O bonds. These peak positions closely align with those reported by other workers in peer-reviewed publications.^{30,31,32}

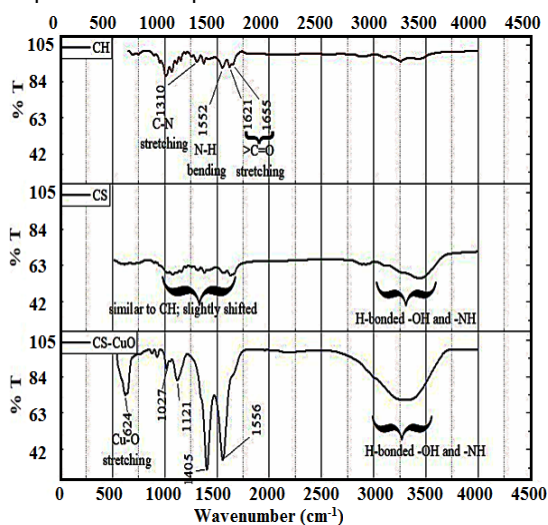


Fig. 2. FTIR spectra for CH (chitin), CS (chitosan), and the CS-CuO nanocomposite

XRD analysis

The XRD spectrum (Fig. 3) shows prominent peaks at 2 θ values: 23.9, 26.4, 29.1, 35.5, 38.9, 43.1, 48.8, 57.1, and 61.62. The peaks at 23.9 and 29.1 correspond to chitosan,^{33,34} whereas the peaks at 35.5°, 38.9°, 43.1°, 48.8°, 57.1°, and 61.62° correspond to the monoclinic structure of CuO nanoparticles as found in tenorite. The sharp peaks at 35.5°, 38.9°, and 48.8° relate to the d-spacing values of 0.25nm, 0.25nm, and 0.18nm respectively, and match closely with JCPDS card number-005-0661, arising from -111, 200, and -202 planes, respectively, of the monoclinic crystal.^{35,36,37} The spectrum is typical of a polycrystalline

substance depicting the incorporation of CuO nanoparticles inside the chitosan matrix. However, another intense peak arising at a 2 θ value of 26.4° can be seen which could be due to unreacted chitin during the deacetylation process which might be present as an impurity.^{38,39} The crystallite size of embedded CuO nanoparticles is 30.34 nm, which has been calculated using the peak at 35.5 with FWHM=0.27484 degrees, through the celebrated Debye Scherrer's equation, $D = k\lambda/\beta\cos\theta$. Here, D symbolizes the size of the crystallite, k and λ denote the Debye Scherrer's constant (0.94) and wavelength of the X-ray source, respectively, and β and θ represent FWHM and angle of incidence respectively.⁴⁰

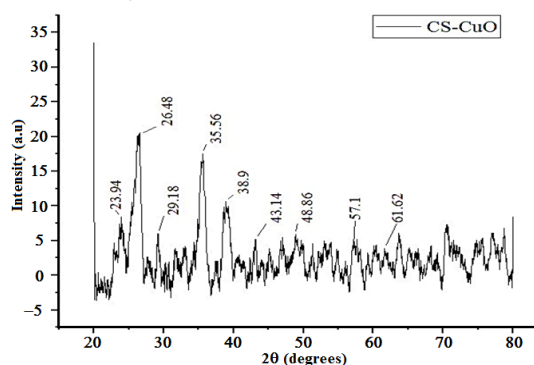


Fig. 3. XRD spectrum of CS-CuO nanocomposite

Morphological analysis through electron microscopy, and SAED

The images obtained through the scanning electron microscope (SEM) show monoclinic crystals of CuO arranged as nanoplates (Fig. 4a). Apparently, the cuboidal particles are stacked together to form plate-like nanostructures. This shows that the CuO crystals possess high purity resulting in self-assembly to higher nanostructures. The thickness of the nanoplates as measured with image J software shows that the plates are of 22.28 nm average thickness. The histogram (Fig. 4b) shows a statistical picture of the thickness distribution between the particles, and it can be easily inferred that most of the nanoplates lie in the same thickness range. The EDS spectrum obtained alongside SEM analysis, shown in Fig. 4c, gives an overview of the elemental composition of the nanocomposite. The copper weight percentage, derived from the intensity values in the EDS plot, is calculated to be 29.09%. The peak observed at 0.28 KeV corresponds to carbon abundance, while

the peaks at 0.4 KeV and 0.53 KeV indicate the respective abundances of nitrogen and oxygen. The peak positioned at 0.9 KeV depicts the binding energy of Cu L, while 8 KeV, and 8.9 KeV are respectively attributed to Cu K α , and Cu K β .⁴¹ The detection of nitrogen, carbon, and oxygen in the EDS analysis supports the findings from other techniques, confirming that chitosan successfully stabilizes the CuO nanoparticles, serving as evidence for the facile synthesis of the CS-CuO nanocomposite. A slight impurity of sulphur can be seen which could be because of traces of sulphate anion from the precursor copper sulphate.

Furthermore, a close inspection of the HRTEM image (Fig. 5a) shows the segregated cuboidal particles dispersed in the chitosan matrix. The segregation is apparently due to higher ultrasonication before TEM imaging as compared to SEM imaging. The SAED pattern (Fig. 5b) obtained during HRTEM analysis also supports the formation of nanocomposite. The concentric rings show the existence of a polycrystalline phase, as is expected from the design of the nanocomposite.⁴²

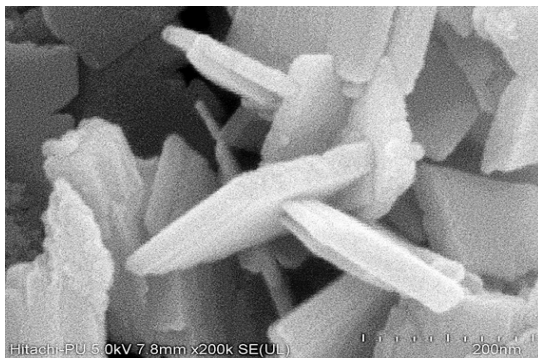


Fig. 4(a). SEM image of CS-CuO nanocomposite

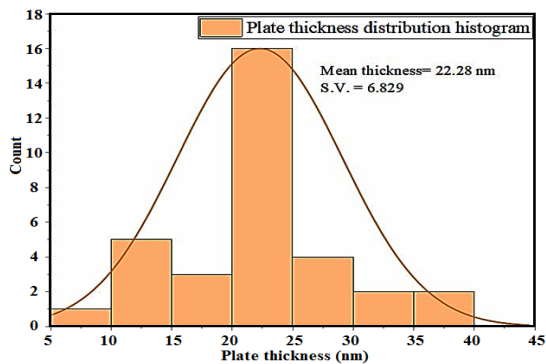


Fig. 4(b). Thickness distribution of nanoplates of CS-CuO nanocomposite

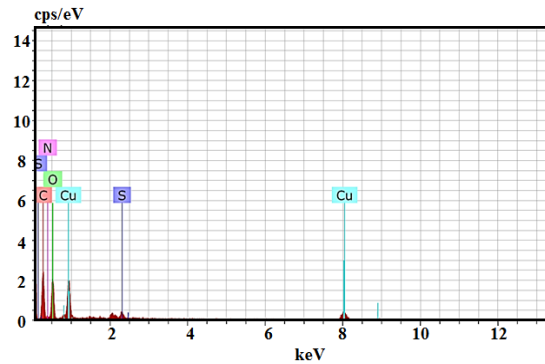


Fig. 4(c). EDS spectrum of the synthesized CS-CuO nanocomposite

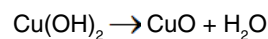
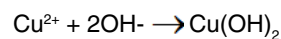


Fig. 5(a). HRTEM image of the synthesized CS-CuO nanocomposite



Fig. 5(b). SAED of the synthesized CS-CuO nanocomposite

A probable step-sequence leading to the formation of CuO nanoplates is shown as follows⁴³:



The CuO thus formed crystallizes as monoclinic crystals, as verified through XRD plot, and undergo self-assembly to form plate-like nanostructures. Since this reaction occurs inside the chitosan matrix, it acts as a stabilizer to limit the growth

of these particles below 100 nm, consequentially forming Chitosan-CuO nanocomposite where CuO is present as nanoplates.

Since this process has been carried out at room temperature using an environmentally benign stabilizer, it represents a greener route for the synthesis of CuO nanoplates, both in terms of energy consumption as well as the use of eco-friendly raw materials. The authors opine that this synthetic route is facile, and can be further explored with slight modifications for the production of Cu nanoparticles

of various morphologies in different oxidation states. The nanoplates fabricated through this method can be investigated for their sensing applications.

ACKNOWLEDGEMENT

This research did not receive any funding from any private, public, or non-profit source.

Conflicts of interest

The authors hereby declare no conflict of interest.

REFERENCES

- Sen, M. Intech Open eBooks. **2020**, <https://doi.org/10.5772/intechopen.93047>
- Phan, T. T. V.; Phan, D. T.; Cao, X. T.; Huynh, T., & Oh., *J. Nanomaterials.*, **2021**, 11(2), 273. <https://doi.org/10.3390/nano11020273>
- Ahmad, W.; Joshi, H.; Ahmed, S.; Kumar, S., & Wilson, I., *Chemical Physics Letters.*, **2024**, 853, 141524. <https://doi.org/10.1016/j.cplett.2024.141524>
- Ahmad, W.; Ahmed, S.; Kumar, S., & Joshi, H. C., *Chemical Papers.*, **2024**, 78(15), 8309–8320. <https://doi.org/10.1007/s11696-024-03669-y>
- Ahmad, W.; Joshi, A.; Kumar, S.; Rana, R.; & Arora, A., *MRS Advances.*, **2023**, 9(12), 970–978. <https://doi.org/10.1557/s43580-023-00715-x>
- Ahmad, W.; Ahmed, S., & Kumar, S., *International Journal of Environmental & Analytical Chemistry.*, **2024**, 1–16. <https://doi.org/10.1080/03067319.2024.2344707>
- He, H. *Elsevier eBooks.*, **2020**, 7-30, <https://doi.org/10.1016/b978-0-12-814930-0.00002-5>
- Živkovi, A., & De Leeuw, N. H., *Physical Review Materials.*, **2020**, 4(7), 074606. <https://doi.org/10.1103/physrevmaterials.4.074606>
- Saad, N. A.; Dar, M. H.; Ramya, E.; Naraharisetty, S. R. G., & Rao, D. N., *Journal of Materials Science.*, **2018**, 54(1), 188–199. <https://doi.org/10.1007/s10853-018-2811-5>
- Flores-Rábago, K. M.; Rivera-Mendoza, D.; Vilchis-Nestor, A. R.; Juarez-Moreno, K., & Castro-Longoria, E., *Antibiotics.*, **2023**, 12(8), 1251. <https://doi.org/10.3390/antibiotics12081251>
- Bezza, F. A.; Tichapondwa, S. M., & Chirwa, E. M. N., *Scientific Reports.*, **2020**, 10(1), 16680. <https://doi.org/10.1038/s41598-020-73497-z>
- Hotze, E. M., Phenrat, T., & Lowry, G. V., *Journal of Environmental Quality.*, **2010** 39(6), 1909–1924. <https://doi.org/10.2134/jeq2009.0462>
- Suryani, S.; Chaerunisaa, A.; Joni, I. M.; Ruslin, R.; Aspadiah, V.; Anton, A.; Sartinah, A., & Ramadhan, L. O. A., *Nanotechnology Science and Applications.*, **2024**, 17, 41–57. <https://doi.org/10.2147/nsa.s450026>
- Scarabelli, L.; Sun, M.; Zhuo, X.; Yoo, S.; Millstone, J. E.; Jones, M. R., & Liz-Marzán, L. M., *Chemical reviews.*, **2023**, 123(7), 3493–3542. <https://doi.org/10.1021/acs.chemrev.3c00033>
- R., Du, J.; Luan, Y.; Xue, Y.; Zou, H.; Zhuang, G., & Li, Z., *Sensors and Actuators B Chemical.*, **2012**, 168, 156–164. <https://doi.org/10.1016/j.snb.2012.03.079>
- Umar, A.; Ibrahim, A. A.; Algadi, H.; Nakate, U. T.; Choudhury, S. P.; Alsuwian, T.; Albargi, H.; Alsaiani, M. A., & Baskoutas, S., *J Mater Sci: Mater Electron.*, **2021**, 32, 18565–18579. <https://doi.org/10.1007/s10854-021-06249-y>
- Alturki, A. M., *Journal of Molecular Structure.*, **2022**, 1263, 133108. <https://doi.org/10.1016/j.molstruc.2022.133108>
- Chen, N.; Liao, Y.; Lin, P.; Chen, W.; Wen, Z.; & Hsieh, S., *International Journal of Molecular Sciences.*, **2021**, 22(23), 12913. <https://doi.org/10.3390/ijms222312913>
- Teli, M., & Sheikh, J., *International Journal of Biological Macromolecules.*, **2012**, 50(5), 1195–1200. <https://doi.org/10.1016/j.ijbiomac.2012.04.003>
- Kumar, M. N. R., *Reactive and Functional Polymers.*, **2000**, 46(1), 1–27. [https://doi.org/10.1016/s1381-5148\(00\)00038-9](https://doi.org/10.1016/s1381-5148(00)00038-9)

21. Gouda, M., & Hebeish, A., *Journal of Industrial Textiles.*, **2009**, 39(3), 203–214. <https://doi.org/10.1177/1528083709103142>
22. Manjunatha, K. B.; Bhat, R. S.; Shashidhara, A.; Kumar, H. S. A., & Nagashree, S., *Journal of Electronic Materials.*, **2021**, 50(6), 3415–3421. <https://doi.org/10.1007/s11664-021-08838-3>
23. Dhineshbabu, N. R.; Rajendran, V.; Nithyavathy, N., & Vetumperumal, R., *Applied Nanoscience.*, **2015**, 6(6), 933–939. <https://doi.org/10.1007/s13204-015-0499-2>
24. Radhakrishnan, A. A., Beena, B. B., *Indian Journal of Advances in Chemical Science.*, **2014**, 2(2), 158-161.
25. Hui, R., & O'Sullivan, M., *Elsevier eBooks.*, **2009**, 1–128. <https://doi.org/10.1016/b978-0-12-373865-3.00001-x>
26. Dahmane, E. M.; Taourirte, M.; Eladlani, N.; & Rhazi, M., *International Journal of Polymer Analysis and Characterization.*, **2014**, 19(4), 342–351. <https://doi.org/10.1080/1023666x.2014.902577>
27. Chen, J.; Zhou, P.; Li, J., & Li, S., *Carbohydrate Polymers.*, **2006**, 67(4), 623–629. <https://doi.org/10.1016/j.carbpol.2006.07.003>
28. Rinaudo, M., *Progress in Polymer Science.*, **2006**, 31(7), 603–632. <https://doi.org/10.1016/j.progpolymsci.2006.06.001>
29. Dillu, E., & Khan, S., *Asian Journal of Chemistry.*, **2024**, 36(10), 2311–2317. <https://doi.org/10.14233/ajchem.2024.32331>
30. Laanoja, J.; Sihtmäe, M.; Vihodceva, S.; Iesalnieks, M.; Otsus, M.; Kurvet, I.; Kahru, A., & Kasemets, K., *Heliyon.*, **2024**, 10(15), e35588. <https://doi.org/10.1016/j.heliyon.2024.e35588>
31. Varughese, A.; Kaur, R., & Singh, P., *IOP Conference Series Materials Science and Engineering.*, **2020**, 961(1), 012011. <https://doi.org/10.1088/1757-899x/961/1/012011>
32. Maheo, A. R.; B, S. M. V., & T, A. a. P., *Results in Surfaces and Interfaces.*, **2022**, 6, 100048. <https://doi.org/10.1016/j.rsufi.2022.100048>
33. Ali, S. A., & Singh, R. P., *Macromolecular Symposia.*, **2009**, 277(1), 1–7. <https://doi.org/10.1002/masy.200950301>
34. Alimatul, N.; Narudin, H.; Mahadi, A. H.; Kusriani, E., & Usman, A., *Materials International.*, **2020**, 2(2), 139–149. <https://doi.org/10.33263/materials22.139149>
35. Rathore, B. S.; Chauhan, N. P. S.; Rawal, M. K.; Ameta, S. C., & Ameta, R., *Polymer Bulletin.*, **2019**, 77(9), 4833–4850. <https://doi.org/10.1007/s00289-019-02994-7>
36. Jain, Y.; Kumari, M.; Laddha, H., & Gupta, R., *Chemistry Select.*, **2019**, 4(23), 7015–7026. <https://doi.org/10.1002/slct.201901355>
37. Narayanan, V. S.; Prasath, P. V.; Ravichandran, K.; Easwaramoorthy, D.; Shahnavaz, Z.; Mohammad, F.; Al-Lohedan, H. A.; Paiman, S.; Oh, W. C., & Sagadevan, S., *Materials Science in Semiconductor Processing.*, **2020**, 119, 105238. <https://doi.org/10.1016/j.mssp.2020.105238>
38. Xin, R.; Xie, W.; Xu, Z.; Che, H.; Zheng, Z., & Yang, X., *International Journal of Biological Macromolecules.*, **2019**, 155, 1561–1568. <https://doi.org/10.1016/j.ijbiomac.2019.11.133>
39. Huet, G.; Hadad, C.; Husson, E.; Laclef, S.; Lambertyn, V.; Farias, M. A.; Jamali, A.; Courty, M.; Alayoubi, R.; Gosselin, I.; Sarazin, C., & Van Nhien, A. N., *Carbohydrate Polymers.*, **2019**, 228, 115382. <https://doi.org/10.1016/j.carbpol.2019.115382>
40. Mobarak, M. B.; Hossain, M. S.; Chowdhury, F., & Ahmed, S., *Arabian Journal of Chemistry.*, **2022**, 15(10), 104117. <https://doi.org/10.1016/j.arabjc.2022.104117>
41. Zayed, M. F.; Eisa, W. H.; Hosam, A. E. M., & Zeid, A. M. A., *Journal of Alloys and Compounds.*, **2020**, 835, 155306. <https://doi.org/10.1016/j.jallcom.2020.155306>
42. Mohan, C.; Kandasamy, R., & Kabiriyel, J., *Carbohydrate Polymer Technologies and Applications.*, **2024**, 7, 100503. <https://doi.org/10.1016/j.carpta.2024.100503>
43. Siriphannon, P., & Iamphaojeen, Y., *Bulletin of the Polish Academy of Sciences.*, **2018**, 66(3). <https://doi.org/10.24425/123437>